PERGAMON

International Journal of Heat and Mass Transfer 44 (2001) 3265–3272

International Journal of HEAT and MASS TRANSFER

www.elsevier.com/locate/ijhmt

Modeling of diffusion filtration combustion radiative burner

Kirill V. Dobrego *, Igor M. Kozlov, Serguei A. Zhdanok, Nikolai N. Gnesdilov

Chemical Physics Laboratory, Heat and Mass Transfer Institute, P. Brovki Street 15, Minsk 220072, Byelorussia

Received 15 September 2000

Abstract

Non-premixed filtration combustion is a new branch of the filtration combustion that combines some properties of turbulent diffusion flames and premixed filtration combustion. Two-dimensional, two-temperature and multi-component model for non-premixed filtration combustion simulation is presented. Parametric study of radiative efficiency of the burner is performed. The lower limit of total equivalence ratio φ for the simulated system is studied parametrically. Simulation predicts high stability of the flame at low equivalence ratios. It is shown that Burke–Schumann combustion and mixing rate well conforms to heat release rate in the non-premixed filtration combustion system.

1. Introduction

Gas combustion in a porous media or filtration combustion (FC) is under intensive investigations now due to a large number of technical applications such as VOCs oxidation, burning lean combustible mixtures under superadiabatic conditions, catalyst treatment by thermal wave, etc. [1,2]. Recently problems of flame front instability, transition between different regimes of the FC and others were addressed [3,4]. In spite of the progress in investigation of FC of premixed fuels the problem of non-premixed FC was not highlighted in the literature. We suppose to use the term filtration combustion in the case when Darcy or Forchheimer filtration hydrodynamics takes place and flame structure is affected by filtration hydrodynamics and interphase heat exchange. Usually this corresponds to small pore size, compared to the flame width (of the order of millimeters). In the opposite case the terms "sinked" flame or "bulked chamber" combustion is more appropriate.

Non-premixed filtration combustion (NFC) is a new area in FC. By analogy with diffusion flames it can be also termed as diffusion filtration combustion. This type of combustion combines some properties of diffusion turbulent flames (high stability and intensity of combustion, flame length conservation, etc.) and of premixed filtration combustion – low NO_x, CO emission level, internal heat recuperation, gas–solid temperature split and others.

One of the possible applications of NFC is radiative burner with controllable heat release and flame length. Since heat release rate is controlled by fuel and oxidant mixing in high temperature systems, the length of the flame L practically does not depend on the gas flow rate. Actually, the length of diffusion mixing is defined by system diameter d_2, gas velocity u_g and diffusivity D. The effective diffusivity has dispersion nature and is proportional to the filtration velocity and porous media particle size $D \sim u_g d_0$ [5] and consequently

$$L \sim \frac{d_2^2 u_g}{D} \sim \frac{d_2^2 u_g}{d_0 u_g} = \frac{d_2^2}{d_0}.$$

In this paper [5] the problem of coaxial gas flux mixing in condition of filtration was considered as a part of a NFC problem. Mixing rate was shown not to depend on total flow rate and variation of the granule size may be utilized for control of heat release rate and flame length. Although heat release rate is in good conformity with simple mixing model, development of the applications such as radiative burner requires more detailed heat and mass transfer simulation with realistic boundary conditions.

* Corresponding author. Tel.: +375-17-284-2021; fax: +375-17-284-2212.

E-mail address: kdob@itmo.by (K.V. Dobrego).

0017-9310/01/$ - see front matter
PII: S0017-9310(00)00343-4

Nomenclature

C_i	molar concentration of the ith gas component
c_i	mass concentration
$\mathbf{D}$	gas diffusivity tensor
$\mathbf{D}_d$	dispersion diffusivity tensor
D_p	longitudinal component of dispersion diffusivity
D_t	transverse component of dispersion diffusivity
D	gas diffusivity coefficient, cm^2/s
d_0	bedding particle diameter, m
d_1	diameter of the internal tube, m
d_2	diameter of the external tube, m
G	gas flow rate, m^3/h
g_1, g_2	parameters in Eqs. (14) and (15)
H	methane heat content, J/kg
$k, \widetilde{k}$	filtration permeabilities
L	burner length, m
M	gas molecular weight, kg/mol
m	porosity
$\mathbf{n}$	normal vector to reactor boundary
Pr	Prandtl number
p	pressure, Pa
p_o	outlet pressure, Pa
R	gas constant
r	system radius, m
r_1	radius of the internal tube, m
r_2	radius of the external tube or radius of the system, m
T	temperature, K
T_0	initial temperature of the system, K
T_{ext}	ambient temperature, K
$\mathbf{u}_g$	filtration velocity vector, m/s

Greek symbols

α_{vol}	heat exchange coefficient, $W/K/m^3$
ε_{int}	emissivity of the imbedded particles
ε_{ext}	emissivity of external tube surface
$\widetilde{\varepsilon}$	gas energy
λ	conductivity, W/m/K
μ	gas viscosity, Pa s
γ	adiabate constant of the gas
φ	equivalence ratio
$\mathbf{\Lambda}$	heat conductivity tensor
ρ	density, kg/m^3
$\dot{\rho}_i$	mass generation of ith component
$\bar{\rho}_i$	mass generation average over cross-section, kg/s/m
σ	Stefan–Boltzmann constant
η	radiative efficiency
$\boldsymbol{\tau}$	normalized velocity vector
τ_z, τ_r	axial and radial components of the velocity vector projection

Subscripts

1	relates to internal tube or fuel
2	relates to external tube or oxidant
g	gas
i	ith component of a gas
s	solid

The aim of this paper is to simulate non-premixed filtration combustion radiative burner, explore the thermal characteristics of the tubular burner with coaxial feed and to demonstrate the possibility of heat release control via two-dimensional simulation.

2. Model of non-premixed filtration combustion burner with coaxial feed

Consider the following model of the non-premixed filtration combustion burner. A gas mixture consisting of different components is pumped through a cylindrical chamber of radius r_2 and length L, filled with the inert fill of porosity m. Gas flow through the chamber is specified by flow rate G at the inlet cross-section ($z = 0$) and pressure p_o at the outlet cross-section ($z = L$) of the chamber. Inlet cross-section is divided into two parts ($r < r_1$) and ($r_1 < r < r_2$) through which gases of different chemical composition (usually fuel and oxidant) and velocity are fed.

$$G = \begin{cases} G_1, & r < r_1, \\ G_2, & r_1 < r < r_2. \end{cases} \tag{1}$$

Gas mixture state and composition are assumed to be defined in arbitrary point by mixture pressure p, gas mixture temperature T_g, mass average velocity $\mathbf{u}_g$ and component concentrations (molar C_i or mass c_i) as well as by the equations of state for the mixture $\rho_g = pM/RT_g$. Average molar mass M is defined through component concentrations $1/M = \sum_i c_i/M_i$.

The carcass state is defined by temperature field T_s. For given carcass temperature field T_s gas parameters are described by stationary equation of continuity

$$\nabla(\rho_g \mathbf{u}_g) = 0 \tag{2}$$

and filtration equation for the gas mixture

$$-\nabla p = \frac{\mu}{k}\mathbf{u}_g + \frac{\rho_g}{\widetilde{k}}|\mathbf{u}_g|\mathbf{u}_g. \tag{3}$$

The above two equations can be reduced to the equation for the pressure

$$\nabla\left(\frac{\nabla p}{(\mu RT_g/Mkp)+(|\mathbf{u}_g|/\widetilde{k})}\right)=0. \tag{4}$$

Equation of mass conservation for each mixture component is

$$\nabla(\rho_g\mathbf{u}_g c_i)-\nabla(\rho_g\mathbf{D}\otimes\nabla c_i)=\dot{\rho}_i, \tag{5}$$

where $\dot{\rho}_i$ is mass generation of ith component due to chemical reactions, to add $\sum_i \dot{\rho}_i=0$; $\mathbf{D}=D_g\mathbf{I}+\mathbf{D}_d$, where $\mathbf{D}_d$ is a dispersion diffusion tensor that depends on gas velocity $\mathbf{u}_g$. It is expressed through longitudinal D_p and transverse D_t components as follows:

$$\mathbf{D}_d=\begin{bmatrix} D_p\tau_z^2+D_t\tau_r^2 & (D_p-D_t)\tau_z\tau_r \\ (D_p-D_t)\tau_z\tau_r & D_p\tau_r^2+D_t\tau_z^2 \end{bmatrix},\quad \boldsymbol{\tau}=\frac{\mathbf{u}_g}{|\mathbf{u}_g|}. \tag{6}$$

Energy equation for a gas

$$c_p\nabla(\rho_g\mathbf{u}_g T_g)-\nabla(\mathbf{\Lambda}\otimes\nabla T_g)=\frac{\alpha_{vol}}{m}(T_s-T_g)-H\dot{\rho}_1 \tag{7}$$

includes heat exchange with the carcass and energy generation due to fuel combustion. Here $\dot{\rho}_1$ is fuel mass consumption at combustion, and $\mathbf{\Lambda}$ is dispersion heat conductivity tensor defined similarly to diffusivity tensor $\mathbf{D}$.

Non-stationary energy equation for carcass includes heat conduction of solid and radiation conductivity components and interphase heat exchange part

$$(1-m)\rho_s c_s\frac{\partial T_s}{\partial t}-\nabla(\lambda\nabla T_s)=\alpha_{vol}(T_g-T_s), \tag{8}$$

$$\lambda=\lambda_s+\frac{16}{3}\left(\frac{0.666m}{1-m}+0.5\right)d_0\varepsilon_{int}\sigma T_s^3 \tag{9}$$

is effective heat conductivity in the carcass.

Boundary conditions. At initial moment gas temperature is assumed equal to T_0. Gas enters the chamber at T_0, so $T_g(z=0)=T_0$. Gas heat exchange with walls is neglected, therefore,

$$(\mathbf{n}\cdot\nabla)T_g=0 \tag{10}$$

on the side surface and at the chamber's outlet cross-section.

Black body irradiation at inlet, outlet cross-section and burner sides is assumed

$$\begin{aligned} -\lambda\frac{\partial T_s}{\partial z}&=\varepsilon_{ext}\sigma(T_s^4-T_0^4), \quad z=0,\\ -\lambda\frac{\partial T_s}{\partial z}&=\varepsilon_{ext}\sigma(T_s^4-T_{ext}^4), \quad z=L,\\ -\lambda\frac{\partial T_s}{\partial z}&=\varepsilon_{ext}\sigma(T_s^4-T_{ext}^4), \quad r=r_2. \end{aligned} \tag{11}$$

The following conditions for pressure are accepted:

Side surface non-permeability.

$$\partial p/\partial r=0,\quad r=r_2. \tag{12}$$

Normal outlet pressure.

$$p=p_0,\quad z=L. \tag{13}$$

The boundary condition for pressure at inlet cross-section ($z=0$) is obtained by using pressure and flow rates G_1, G_2 compliance condition

$$\partial p/\partial z=\begin{cases} g_1 & \text{for } r<r_1,\\ g_2 & \text{for } r_1<r<r_2, \end{cases}$$

where

$$g_1\int_0^{r_1}\frac{r\,dr}{(\mu RT_g/Mkp)+(|\mathbf{u}_g|/\widetilde{k})}=-\frac{\rho_{01}G_1}{\pi m},\quad r<r_1, \tag{14}$$

$$g_2\int_0^{r_1}\frac{r\,dr}{(\mu RT_g/Mkp)+(|\mathbf{u}_g|/\widetilde{k})}=-\frac{\rho_{02}G_2}{\pi m},\quad r_1<r<r_2. \tag{15}$$

Wall non-permeability is applied for the gas components, Eq. (5)

$$(\mathbf{n}\cdot\nabla)c_i=\begin{cases} 0 & \text{for } r=r_2,\\ 0 & \text{for } z=L. \end{cases} \tag{16}$$

Initial composition of gases is specified in the inlet cross-section, i.e.

$$c_i(z=0)=\begin{cases} c_{i1}, & r<r_1,\\ c_{i2}, & r_1<r<r_2. \end{cases} \tag{17}$$

To prevent uncontrollable diffusion and energy flow through the inlet cross-section, we assume

$$\mathbf{D}(z=0)=0,\quad \mathbf{\Lambda}(z=0)=0. \tag{18}$$

3. Results and discussion

For numerical simulation the following primary parameters were accepted: volumetric heat exchange coefficient [6]:

$$\alpha_{vol}=\frac{\lambda_g 6(1-m)}{d_0^2}\left[2+1.1Pr^{1/3}\left(\frac{\rho_g u_g d_0}{\mu}\right)^{0.6}\right]; \tag{19}$$

permeabilities [7]: $k=(d_0^2m^2/150(1-m)^2)$, $\widetilde{k}=(d_0m/1.75(1-m))$. Nitrogen diffusion, viscosity and heat conduction coefficients were used for gas phase. The following approximations with characteristic accuracy better than 5% in all temperature range were utilized: $D_g=0.18(T/273)^{1.75}(p_o/p)$ cm^2/s; $p_o=1.013\times10^5$ Pa; $\lambda_g=1.4\times10^{-2}+4.8\times10^{-5}T$, W/m/K; $\mu=4.4\times10^{-7}T^{0.65}$ Pa s. The first-order brutto kinetics often used for FC modeling [8] is not applicable for non-premixed combustion simulation. For this reason we used the

second-order methane oxidation kinetics which was fitted to satisfy normal flame propagation velocity at atmospheric pressure $d[CH_4]/dt = -3.6 \times 10^{-10}[CH_4][O_2]\exp(-15640/T)$, here concentrations $[CH_4]$ and $[O_2]$ have dimension cm^{-3}. Other parameters: solid emissivity $\varepsilon_{ext} = 0.4$, $\varepsilon_{int} = 0.4$; tube length $L = 0.3$ m; burner diameter $d_2 = 0.038$ m; internal tube diameter $d_1 = 0.023$ m; outlet pressure, $p_o = 1.013 \times 10^5$ Pa, porosity $m = 0.4$; gas molecular weight $M = 0.029$ kg/mol; bedding particle diameter $d_0 = 0.003$ m; methane heat content $H = 5.3 \times 10^7$ J/kg; porous media heat conduction coefficient $\lambda_s = 0.2$ J/m/K; longitudinal and transverse dispersion diffusivity

$$D_p = 0.5 d_0 u_g, \quad D_t = 0.1 d_0 u_g. \tag{20}$$

In the standard case volumetric flow rates of methane and air were as follows: $G_1 = 0.2$ and $G_2 = 2$ m^3/h, which corresponds to equivalence ratio $\varphi = 0.95$, concentration of methane at inlet is unity, concentration of oxygen in air is 0.21.

Ignition of the burner was simulated with the temperature initial distribution. The temperature of the 3 cm end portion of the carcass was 1200 K and the temperature of the rest part of carcass was 300 K. The physical time which was necessary to reach thermal steady state varied from 20 to 90 min, depending on flow

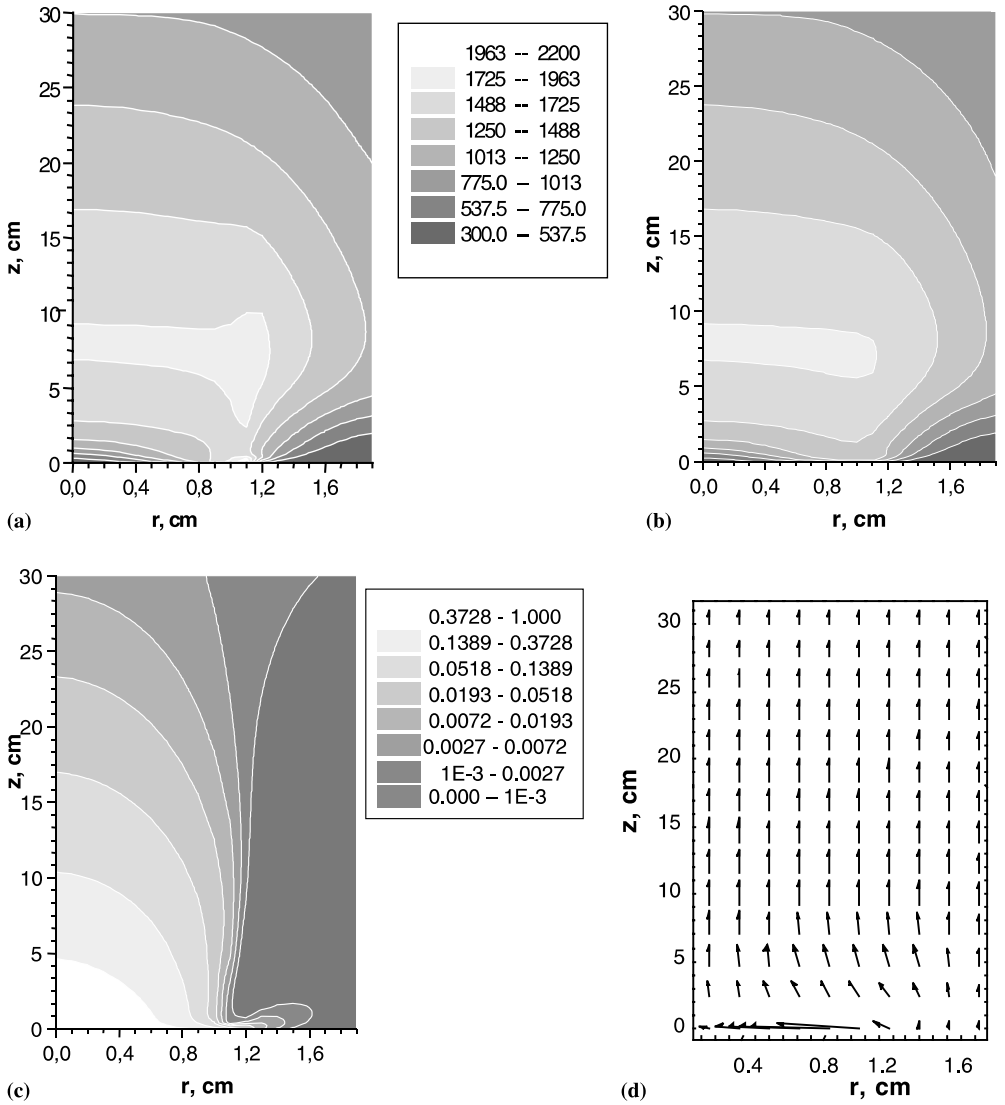

Fig. 1. Stationary temperature field of gas (a) porous media (b) methane dimentionless concentration (c) and filtration velocity field (d) as calculated for standard case parameters and free irradiation from the burner side surface.

rates and mixture equivalence ratio. Temperature, concentration and filtration fields calculated for the standard case are presented in Fig. 1. The calculations show that temperature difference between gas and solid is higher than in the case of premixed filtration combustion and may reach 200–300 K. In the area aside of the maximal heat release the gas and solid temperature fields are quite similar. On the graph in Fig. 1(c) the splash of methane concentration at the beginning of the burner is seen. This is due to the fact that dispersion provides high diffusivity for the gas at the time the temperature is not enough high to secure instantaneous methane burning out at the mixing. Fig. 1(d) demonstrates that the filtration field may be very inhomogeneous at the beginning of the burner, but quickly relax to uniform one at the length of the order of one tube diameter. To analyze heat release intensity by the length of the burner, we calculated local methane consumption rate, $\dot{q}_1$, Fig. 2. The logarithmic scale was applied to visualize low level effects. Calculations demonstrate that heat release zone is rather narrow and its location very slightly depends on total flow rate at the given equivalence ratio which is a proof of the diffusion character of the flame.

The radiative efficiency of the system $\eta = Q_{\text{rad}}/Q_{\text{tot}}$ is defined as a ratio of irradiated energy from the surface to the total firing power. It is one of the most important parameters in the case of the radiative burner application. It was calculated as a function of the total flow rate at fixed equivalence ratio, Fig. 3, and as a function of methane flow rate at fixed air flow rate, Fig. 4. As follows from Fig. 3, the efficiency grows while total flow rate decreases. High value of the efficiency indicates very effective heat exchange and transportation from the reaction zone to the irradiating surface. Low efficiency at

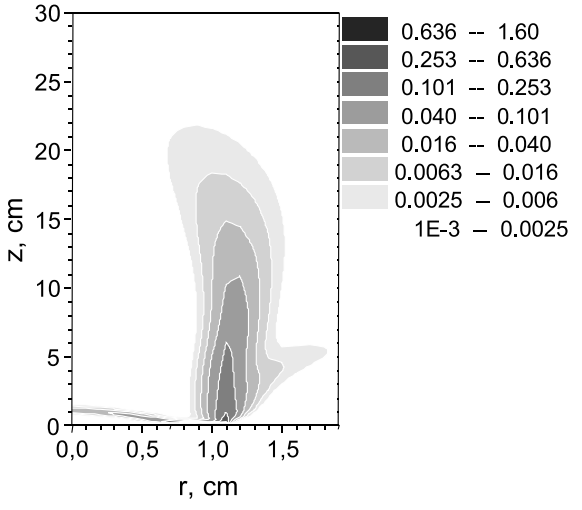

Fig. 2. Local methane consumption rate $\dot{q}_1$, kg/s/m^3, in the burner. Logarithmic scale presentation.

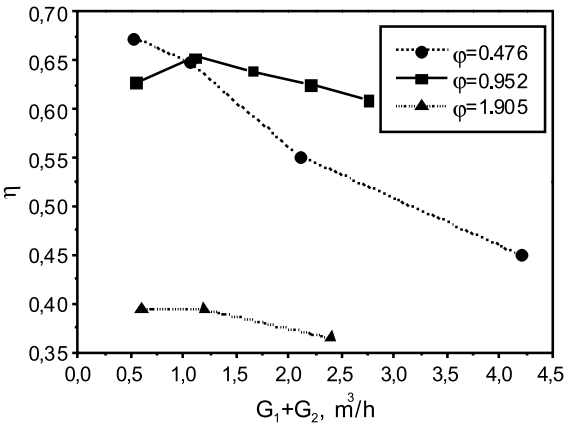

Fig. 3. Radiative efficiency of the burner as a function of total flow rate calculated for different equivalence ratios, as presented in the legend.

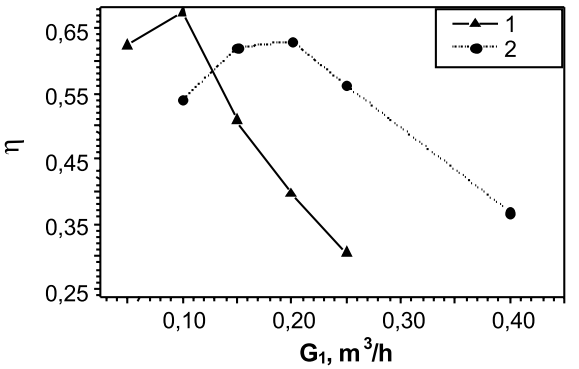

Fig. 4. Radiative efficiency of the burner as a function of methane flow rate at fixed air flow rate, as presented in the legend. Line 1 – $G_1 = 1$ m^3/h, line 2 – $G_2 = 2$ m^3/h.

$\varphi = 1.905$ is explained by incomplete fuel combustion. The observed (in Fig. 3) reduction of the efficiency at low flow rates is due to incomplete burning out in condition of considerable heat losses. In the case of low equivalence ratio of $\varphi = 0.476$ this effect is not exist. The efficiency peaks in Fig. 4 corresponds to the stoichiometric air–fuel mixture.

A parametric study of the radiative efficiency was performed in which the internal tube diameter and bedding particle diameter were varied. In Fig. 5 radiative efficiency presented as a function of the inner tube radius at fixed flow rates $G_1 = 0.2$ m^3/h, $G_2 = 2.0$ m^3/h. The smaller inner tube corresponds to smaller radius of the heat release zone and consequently higher time of heat transfer from heat release zone to radiating surface. We expected some increase if the efficiency with the internal tube radius growth. Calculations demonstrate slight decrease of efficiency with the radius growth. This kind

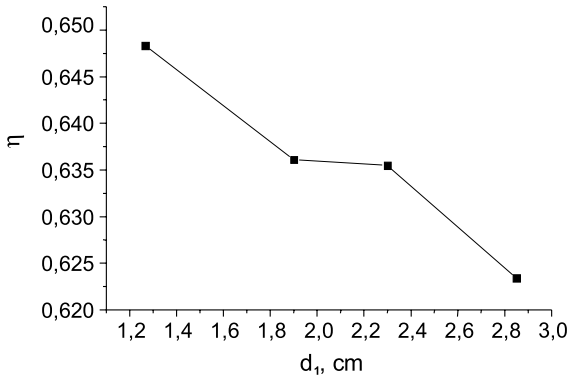

Fig. 5. Radiative efficiency dependence on the inner tube radius at fixed flow rates $G_1 = 0.2$, $G_2 = 2.0$ m^3/h.

of behaviour of the system is explained by incomplete fuel combustion.

The results of calculation of radiative burner efficiency as a function of the bedding particle diameter are presented in Fig. 6. One can see the maximum on the graph corresponding to the particle size $d_0 \approx 4$ mm. This result shows that choosing optimum particle distribution may provide 2–4 percent of total efficiency of the system. Existence of the maximum may be explained in the following. Small particles corresponds to smaller hear transfer coefficient (dispersion plus radiation) and cannot provide complete transportation of the energy from reaction zone to the walls. At the same time big particle do not provide high gas-to-solid transfer coefficient, and consequently combustion products take away some more heat.

Another parameters important for radiative burner design is surface temperature distribution and heat release rate along the burner. Heat release rate may be obtained with Burke–Schumann solution [9] for the diffusion flame. As shown in [5] even the first term in the exponential series of the Burke–Schumann solution gives good approximation for the mixing and combustion rate averaged over cross-section at coaxial feed. The corresponding fuel consumption rate $\bar{\rho}_1 = a(1 - \exp(-14.66 d_0 x/r_2^2))$, a = normalization constant, is presented in Fig. 7 with dotted line. The same parameter was obtained numerically for two total flow rates $G = 2.2$ and $G = 1.1$. Good agreement between Burke–Schumann one-exponent correlation and numerical solution for methane consumption is observed. Naturally, fuel combustion does not start from the very beginning of the burner (as Burke–Schumann model assumes) and the peak of fuel consumption lies in coordinate $x \approx 3$ to 4 mm. Another difference is related to fuel consumption slowdown at coordinate $x = 2$ to 4 cm, this corresponds to local combustion intensification observable in Fig. 2. The temperature of the external boundary of the burner calculated numerically is presented on the same graph. It is seen that surface temperature distribution does not correlate to the heat release rate directly and vary with flow rate due to complex nature of heat transfer from the reaction zone to the irradiating surface. The results obtained confirmed general understanding of the process. The mixing and heat release rates are not significantly affected by flow rate variation. Surface temperature profile is shifted in the direction of filtration, maximum surface temperature and temperature variation at the length of working part of the radiative burner (~25 cm) is increased in the case of higher flow rate. The surface temperature profile shift is undesirable effect from the viewpoint of radiative burner design as far as it limits firing power range. Numerical simulation shows that this effect may be compensated with inner tube diameter increase or interchange of fuel and air feed channels.

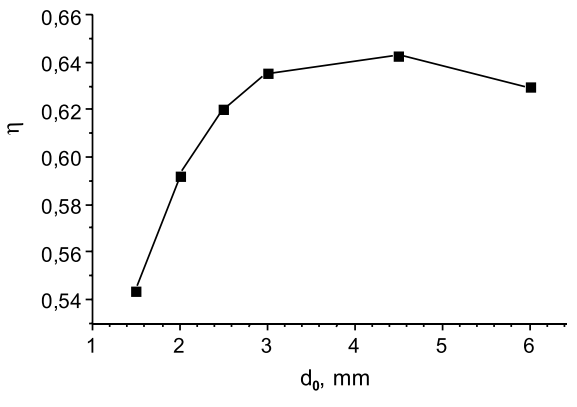

Fig. 6. Radiative efficiency dependence on the bed particle diameter d_0. $G_1 = 0.2$, $G_2 = 2.0$ m^3/h.

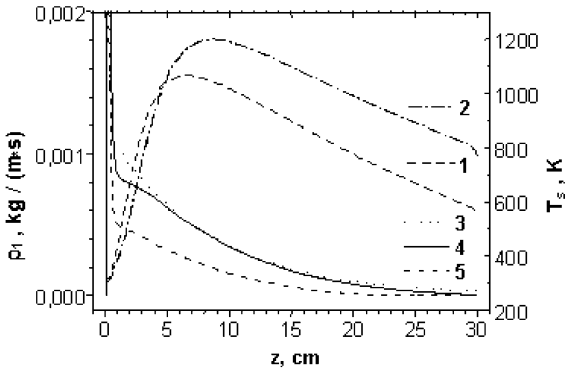

Fig. 7. Burner surface temperature (lines 1 and 2) and methane consumption rate averaged by cross-section (lines 5 and 4) calculated for total flow rates $G = 1.1$ and $G = 2.2$ m^3/h, respectively. Line 3 presents one-exponent Burke–Schumann estimate for methane consumption for $G = 2.2$ m^3/h.

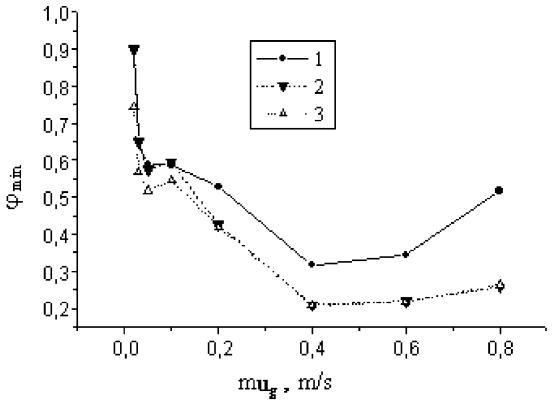

Fig. 8. Dependence of φ_{min} on superficial gas velocity $m\mathbf{u}_g$ with different bedding particle diameter d_0 and ambient temperature T_{ext}. (1) $d_0 = 3 \times 10^{-3}$ m, $T_{ext} = 300$ K, (2) $d_0 = 1 \times 10^{-3}$ m, $T_{ext} = 300$ K, (3) $d_0 = 3 \times 10^{-3}$ m, $T_{ext} = 500$ K. $d_1 = 2 \times 10^{-2}$, $d_2 = 4 \times 10^{-2}$ m is constant.

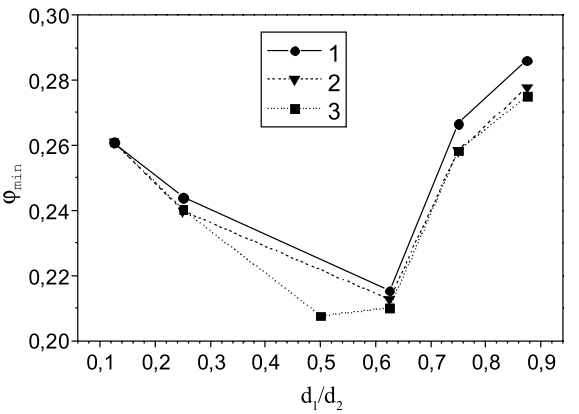

Fig. 10. Dependence of φ_{min} on d_1/d_2 with different bedding particle diameter d_0. (1) $d_0 = 3 \times 10^{-3}$ m, $T_{ext} = 300$ K, (2) $d_0 = 3 \times 10^{-3}$ m, $T_{ext} = 300$ K without irradiation from end-wall, (3) $d_0 = 1 \times 10^{-3}$ m, $T_{ext} = 300$ K. $d_2 = 4 \times 10^{-2}$ m and $m\mathbf{u}_g = 0.4$ m/s is constant.

We also examined the lean limits of stable combustion in the given system. The lean limit was characterized via minimal value of total equivalence ratio providing stationary combustion in the system and was defined by numerical simulation. The length of the simulated system was $L = 15$ cm. Superficial gas velocity $m\mathbf{u}_g$, diameter of the internal and external tubes d_1 and d_2, bedding particles diameter d_0 and ambient temperature T_{ext} were varied. Emissivity of external tube and porous carcass were accepted $\varepsilon_{ext} = 0.3$, $\varepsilon_{int} = 0.3$, respectively. Ignition of the system was simulated by heating up of the burner to the temperature of 1200 K. The results of this investigation are presented in Figs. 8–10.

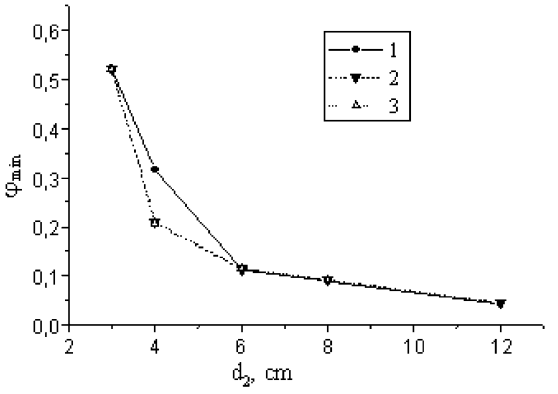

Fig. 9. Dependence of φ_{min} on external tube diameter of d_2 with different bedding particle diameter d_0 and ambient temperature T_{ext}. (1) $d_0 = 3 \times 10^{-3}$ m, $T_{ext} = 300$ K, (2) $d_0 = 1 \times 10^{-3}$ m, $T_{ext} = 300$ K, (3) $d_0 = 3 \times 10^{-3}$ m, $T_{ext} = 500$ K. $d_1/d_2 = 0.5$, $m\mathbf{u}_g = 0.4$ m/s is constant.

The dependence of φ_{min} on superficial gas velocity $m\mathbf{u}_g$ is presented in Fig. 8. Bedding particle diameter d_0 and ambient temperature T_{ext} were varied. Tubes diameters were $d_1 = 2 \times 10^{-2}$, $d_2 = 4 \times 10^{-2}$ m. The graph has a minimum at $m\mathbf{u}_g \sim 0.4$ m/s. This explained by competition of the process of fuel and oxidant mixing according to Eqs. (5) and (6) and heat loses from combustion front Eqs. (7)–(9), (11) and (19). With $m\mathbf{u}_g$ increase, intensity of mixing fuel and oxidant grows up, that, in its turn, decreases φ_{min}. On the other hand, $m\mathbf{u}_g$ increase leads to higher heat exchange rate and thus to higher heat loses from combustion front. As shown in Fig. 8, the smaller bed particles diameter d_0 and lower T_{ext} corresponds to lower φ_{min}.

The dependence of φ_{min} on the diameter of external tube d_2 for the cases of different bedding particle diameters d_0 and ambient temperature T_{ext} is presented in Fig. 9. The tube 1 to tube 2 diameters ratio and gas velocity were as follows $d_1/d_2 = 0.5$, $m\mathbf{u}_g = 0.4$ m/s. The trends of the graph are explained as follows. With the d_2 increase, combustion takes place farther from the surface, heat loses decrease which results in lower value of φ_{min}. At $d_2 \geqslant 6$, value of φ_{min} does not depend on d_0 and T_{ext} noticeably.

In Fig. 10 the φ_{min} as a function of d_1/d_2 is presented. The external tube diameter $d_2 = 4 \times 10^{-2}$ m and $m\mathbf{u}_g = 0.4$ m/s were taken constant. The cases of different particle diameters d_0 were simulated.

4. Conclusions

Non-premixed filtration combustion is characterized with considerable split between the gas phase and solid

temperature which reaches 200–300 K in the simulated conditions and higher than the one in premixed filtration combustion systems at the same equivalence ratio and total flow rate. This effect may be utilized for implementation of high temperature gas phase chemical processes.

Simulation of NFC predicts high stability of the flame at low equivalence ratios. The proper geometry of the fuel–air feed provides the lower limit of $\varphi \approx 0.2$ for stable combustion for the simulated system.

Burke–Schumann mixing rate conforms well to heat release rate in the NFC system, although surface temperature distribution and heat transfer inside the system should be calculated with 2D model.

Acknowledgements

This research was partially sponsored by Fond for Fundamental Research of Republic of Belarus, grant T98-209.

References

[1] J.R. Howell, M.J. Hall, J.L. Ellzey, Prog. Energy Combust. Sci. 22 (1966) 122–145.
[2] L.A. Kennedy, A.A. Fridman, A.V. Saveliev, J. Fluid Mech. Res. 22 (2) (1996) 1–26.
[3] K.V. Dobrego, S.A. Zhdanok, A.V. Krauklis, J. Eng. Phys. Thermophys. 72 (1999) 440–449.
[4] S.A. Zhdanok, K.V. Dobrego, Combustion, Explosion and Shock Waves 35 (1999) 650–656.
[5] K.V. Dobergo, V.I. Kalinin, V.A. Zhdanok, I.M. Kozlov, in: Proceedings of the Third International School-Seminar Modern Problems of Combustion, HMTI Publications, Minsk, August 1999, pp. 26–30.
[6] N. Wakao, S. Kaguei, in: Heat and Mass Transfer in a Packed Beds, Gordon and Breach, New York, 1982.
[7] A. Amiri, K. Vafai, Int J. Heat Mass Transfer 37 (1994) 939–954.
[8] S. Foutko, S. Zhdanok, S. Shabunia, in: Proceedings of the 26th Symposium International on Combustion, The Combustion Institute, Pittsburgh, vol. 2, 1992, p. 222.
[9] Ya.B. Zeldovich, G.I. Barenblatt, V.B. Librovich, G.M. Machviladze, in: The Mathematical Theory of Combustion and Explosions, Plenum, New York, 1985.